

A birefringence correction for multi-frequency radar sounding

Benjamin H. Hills^{ID} Matthew R. Siegfried^{ID} Duncan A. Young^{ID} John D. Paden^{ID} Shivangini Singh^{ID}
Colorado School of Mines Colorado School of Mines University of Texas University of Kansas University of Texas
Golden, CO, USA Golden, CO, USA Austin, TX, USA Lawrence, KS, USA Austin, TX, USA
benjamin.hills@mines.edu siegfried@mines.edu duncan@ig.utexas.edu paden@ku.edu shivangini@utexas.edu

Donald D. Blankenship^{ID}
University of Texas
Austin, TX, USA
blank@ig.utexas.edu

Dustin M. Schroeder^{ID}
Stanford University
Palo Alto, CA, USA
dustin.m.schroeder@stanford.edu

Abstract—An ice crystal has uniaxial symmetry about its *c* axis and is therefore electrically anisotropic. Anisotropy in the real dielectric permittivity at radio wavelengths means that ice is birefringent to radar waves, including those commonly used to sound through ice masses. Radar birefringence can be targeted as a measurement signal to interpret ice anisotropy for ice rheology or ice-flow history; however, birefringent losses can also act as noise when targeting the reflected radar power as a measure of interface properties or attenuation. Here, we propose a method for correcting birefringent losses in multi-frequency radar sounding. Birefringent loss fringes occur at a regular interval that depends on the center frequency of the transmitted signal, so correlating loss fringes from radar systems with different frequencies enables a more precise and robust estimate of electrical anisotropy, which can then be used as a correction for birefringent power losses. We demonstrate our method with an example from a dual-frequency instrument recently used for sounding the Antarctic Ice Sheet. We choose an example where the loss fringes are visible within the specular englacial layers, but we argue that our correction method is useful even for a single diffuse reflector where the loss fringes may be obscured by variations in the reflector properties. Similar birefringent correction methods can be applied to planetary radar sounding cases, such as the two radar sounders orbiting Mars or the dual-frequency radar instrument onboard the Europa Clipper.

Index Terms—IGARSS 2025, radar sounding, birefringence, ice-sheet anisotropy.

I. INTRODUCTION

Ice masses, such as glaciers and ice sheets, are made up of many individual ice crystals of varying size, shape, and orientation, together forming the bulk crystal orientation fabric (COF) [1]. On Earth’s surface, and for the planetary water ice masses that we know of, the individual crystals have a hexagonal basal plane and orthogonal *c* axis, a molecular structure called ice Ih [2]. The electrical properties of the ice-Ih crystal are unique depending on its orientation [3]; for example, at radio wavelengths, the real permittivity is ~1% larger (slower wave speed) when the wave is polarized in line with the *c* axis than across [4, 5]. In other words, the crystal

is electrically anisotropic or “birefringent”, and an ice mass can inherit a bulk anisotropy if its COF consists of aligned crystals. Ice masses are commonly anisotropic since COFs evolve toward preferred directions as ice flows [6]. Measured COFs can therefore be used to interpret ice-flow history [7, 8] and can help predict future ice-flow behavior caused by COF-induced mechanical anisotropy [9, 10].

COF in glaciers and ice sheets can be measured indirectly and remotely with radar sounding [11]. A radar wave depolarizes as it propagates through anisotropic ice, so a measured polarization difference between the transmitted and received waveforms can be attributed to birefringence in the ice column. There are specific polarimetric survey strategies that target birefringence [11, 12], but the signals can also manifest as a radar power loss [13] even in the conventional *non-polarimetric* radar surveys that cover much of the Greenland and Antarctic ice sheets [14, 15]. Although birefringent power losses can theoretically be corrected as a term in the radar power equation [16], they are rarely considered in other analyses of radar power such as attenuation or reflectivity. Whether in a polarimetric or conventional survey, the birefringent signatures depend on frequency of the transmitted signal. Radar sounders are generally designed in the broad frequency band from HF to UHF ($\sim 10^6$ – 10^9 Hz) for which ice is non-dispersive and non-absorptive [3, 17]. Higher frequency radars with a large bandwidth give superior range resolution for distinguishing annual stratigraphy in the near-surface snow/firn [18], and lower frequency radars propagate to deeper depths in the ice with less attenuation.

Here, we describe the frequency dependence of birefringent signatures in non-polarimetric radar sounding surveys and provide a power correction for the associated power losses which can be used in multi-frequency systems. We first provide the theoretical background on how birefringent signatures manifest in non-polarimetric surveys, then show an example with a dual-frequency system in East Antarctica that expresses different birefringent signatures for each transmitted frequency. We argue that, for co-deployed multi-frequency

TABLE I
LIST OF ALL VARIABLE DEFINITIONS USED IN THIS WORK.

x, y, z	spatial dimensions
t	time
ψ	azimuth angle
ϵ_r	relative permittivity
$\Delta\epsilon_r$	change in permittivity (effective anisotropy)
f_c	center frequency
v_{fs}	wave velocity in free space
ϕ	phase
γ	rotation of polarization ellipse
Ω	beat frequency
L	beat wavelength
H	horizontally polarized wave component
V	vertically polarized wave component

radars, we can use the differences between birefringent signatures to increase our confidence in the interpretation of anisotropy and correct for birefringent losses in each system. We propose our own algorithm for birefringence corrections and discuss how it may be used in both terrestrial and planetary applications.

II. BACKGROUND - THE BIREFRINGENT BEAT

To discuss birefringence and the associated power losses in non-polarimetric radar surveys, we first give a brief background on the nature of polarized wave propagation through anisotropic media. For a plane wave, the complex electric field amplitude can be described as a Jones vector [19] for which the wave components, H and V , can be combined to yield the equation for an ellipse [20] traced out over time, $t = 1/f_c$, where f_c is the instrument center frequency. The wave is therefore elliptically polarized. The shape of this polarization ellipse can be described with two variables, a phase delay

$$\phi_{\text{ellipse}} = \arg(H \cdot V^*), \quad (1)$$

and a rotation

$$\gamma = \tan^{-1} \left(\frac{|V|}{|H|} \right), \quad (2)$$

where $*$ is the complex conjugate. At $|H| = 1$ the wave polarization is unrotated (linear polarization in the x direction) and at $|V| = 1$ it is fully rotated (linear polarization in the y direction). If the receive antenna is also polarized, it will selectively measure the electric field from the wave component that aligns with it. When a polarized wave propagates through anisotropic media, the polarization ellipse changes shape with propagated distance, and the component rotated out of view of the antenna appears to go missing as a birefringent power loss.

Full consideration of wave depolarization in anisotropic media uses transfer matrices to update the Jones vector [11, 21]. Here though, we only consider power losses and in particular the “beat frequency” or periodicity of the birefringent loss signature. Rotation of the polarization ellipse stems from the differential wave speed between orientations which creates a phase delay between orthogonally polarized wave components. Following the assumptions of Jordan et al. [22], for small

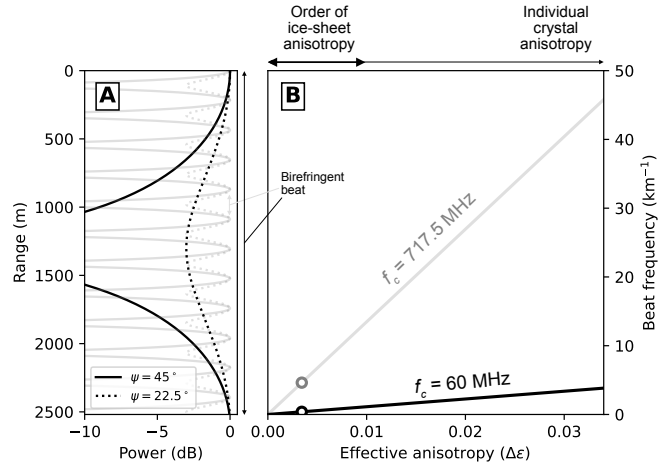


Fig. 1. Theoretical expression of the birefringent beat signature in ice with constant anisotropy and for two radar instruments with center frequencies 60 MHz (black) and 717.5 MHz (gray). A) Power returned to the radar receiver for a wave initially polarized 45° (solid) or 22.5° (dotted) from the COF principal axes. B) Beat frequency calculated with equation (4), with open circles indicating the effective anisotropy used in (A).

deviations about a mean (polarization-averaged) permittivity, the two-way phase delay is

$$\phi = \frac{2\pi f_c}{v_{fs} \sqrt{\epsilon_r}} \int_{z_0}^{z_1} \Delta\epsilon_r(z) dz, \quad (3)$$

where v_{fs} is the free-space velocity, ϵ_r is the bulk relative permittivity, and $\Delta\epsilon_r$ is the effective anisotropy that the wave is subjected to. Considering vertically propagating plane waves, $\Delta\epsilon_r$ can only change in z .

The beat frequency is then calculated as the depth gradient in phase divided by 2π radians per wavelength. Within a layer of uniform anisotropy, the integral in equation (3) reduces to $z\overline{\Delta\epsilon_r}$, so the beat frequency is

$$\Omega = \frac{f_c \overline{\Delta\epsilon_r}}{v_{fs} \sqrt{\overline{\epsilon_r}}}, \quad (4)$$

with units m^{-1} , where $\overline{\Delta\epsilon_r}$ and $\overline{\epsilon_r}$ are the depth-averaged dielectric anisotropy and permittivity, respectively, and $L = 1/\Omega$ is the associated beat wavelength. The extent of rotation of the polarization ellipse, i.e., maximum change in γ , depends on the degree of misalignment from the principal axes. At maximum misalignment, $\psi = \frac{(2n+1)\pi}{4}$, the wave is *fully* rotated and a power minimum is seen in the copolarized acquisition. At maximum alignment, $\psi = \frac{n\pi}{2}$, the wave is unrotated, no birefringent losses are observed, and a cross-polarized antenna receives no power (cross-polarized extinction). Unlike the magnitude, the *frequency* of the beat is independent of azimuth, so in cases where: i) the radar antennas are misaligned from the ice anisotropy, ii) the beat can be distinguished from repeated reflecting horizons, and iii) the ice is sufficiently thick for multiple beats to be observed, this phenomena can be quantified.

Equation (4) has a dependence on the instrument center frequency, so the beat signature manifests differently between

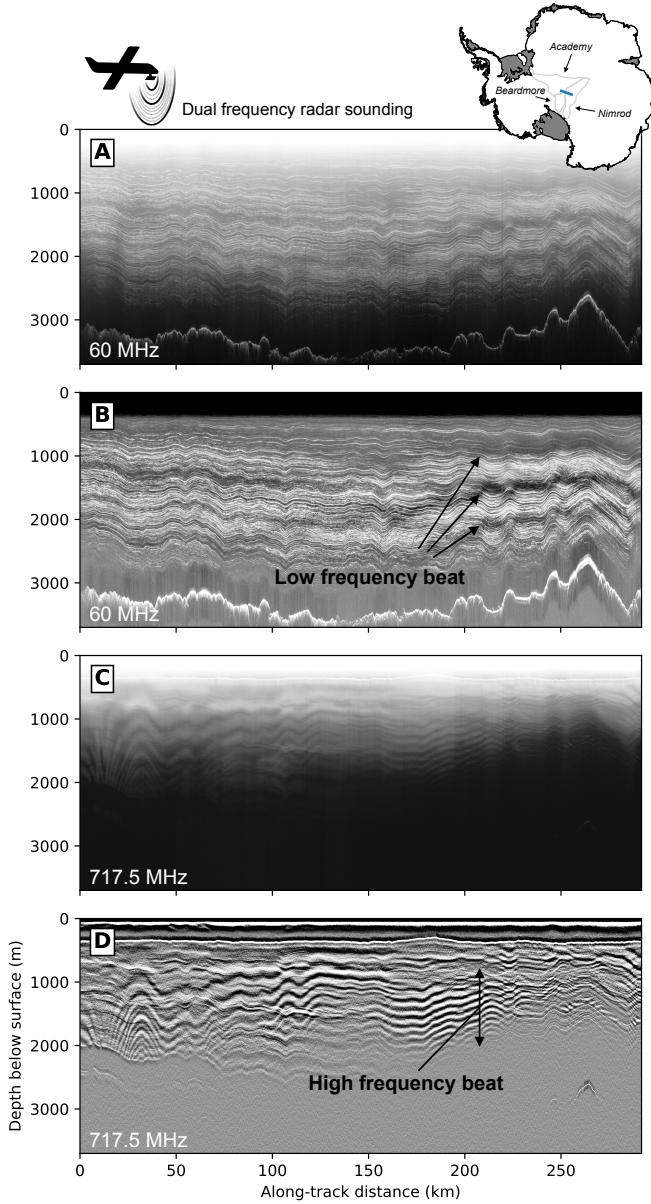


Fig. 2. Z-scope radar images from two separate instruments with (A, B) 60 MHz and (C,D) 717.5 MHz center frequencies. Both instruments were mounted on the same aircraft, so they were acquired simultaneously. We show both the pulse-compressed image (A, C) and a high-pass filtered image (B, D) to highlight the birefringent beat. Inset map shows Antarctic coastline and grounding line with drainage basins for the relevant glaciers (Academy, Beardmore, and Nimrod) and a blue line for the flight track.

radar systems. Multi-frequency systems could therefore be designed to potentially overcome requirements (ii) and/or (iii) or to correct the birefringent losses entirely.

III. AN EXAMPLE FROM THE ANTARCTIC ICE SHEET

As a demonstration of multi-frequency birefringence, we use data from the 2023–24 Antarctic airborne radar mission by the Center for Oldest Ice Exploration (COLDEX), which was flown with two radar instruments onboard the same aircraft to resolve different targets simultaneously [23].

The first instrument is the University of Texas Institute for Geophysics (UTIG) Multifrequency Airborne Radar Sounder with Full-phase Assessment (MARFA). MARFA has 60 MHz center frequency and 15 MHz bandwidth, targeting the ice-bed interface and deep englacial layers. The second is the Center for Remote Sensing and Integrated Systems (CReSIS) accumulation radar. This CReSIS radar has 717.5 MHz center frequency and 60 MHz bandwidth, targeting the shallower englacial layers and with finer range resolution. The transmit and receive antennas are co-polarized for each, but the two systems are perpendicular to one another.

The airborne survey broadly covers the region between South Pole and Dome A, with the objective to find a glaciological setting which may preserve old ice [24]. The selected flight track in Figure 2 is along 110°E longitude, crossing the continental ice divide between Beardmore and Nimrod glaciers (which flow into the Ross Ice Shelf) and Academy Glacier (which flows into the Filchner Ice Shelf). Ice velocities are slow in this area (order 1 m/yr), so the anisotropy in present-day ice would have taken centuries or millennia to develop.

The birefringent beat is visible at both instrument frequencies. In places where anisotropy is weak (e.g., at ~10 km along-track distance) the beat is not well resolved by the lower frequency system since the beat wavelength approaches the full ice thickness. On the other hand, when the anisotropy is strong (~260 km along track) the low-frequency beat is better distinguished and the high-frequency beat is difficult to distinguish among the reflectivity variations. In this way, the two beats in a dual-frequency system are complementary measurements.

IV. A MULTI-FREQUENCY CORRECTION FOR BIREFRINGENT LOSSES

The birefringent beat is commonly used itself as a *signal* for interpretations of ice anisotropy [25, 26], but it is also a loss term in the radar power equation [13]. In theory, one could correct for birefringent losses with a model of the ice anisotropy, but in practice such an effort is difficult since it requires a precise knowledge of the past and present ice flow. Otherwise, corrections are plausible where an ice core has been drilled and the ice sampled directly, but extending that correction would require an assumption for how the anisotropy changes away from the of observation. Instead, a more viable birefringence correction uses multiple independent geophysical measurements at distinct frequencies, removing the circularity of using a signal to correct itself. Knowing that each waveform interacts with the same ice, the only free variable in equation 4 is the center frequency, so any additional measurements at variable frequency add confidence for noisy signals.

We add our correction into the standard processing pipeline (Figure 3). To extract the cleanest beat signature, we first average traces incoherently within a moving aperture. This averaging decreases the coherent signal for reflecting horizons (englacial layers) while maintaining the incoherent magnitude

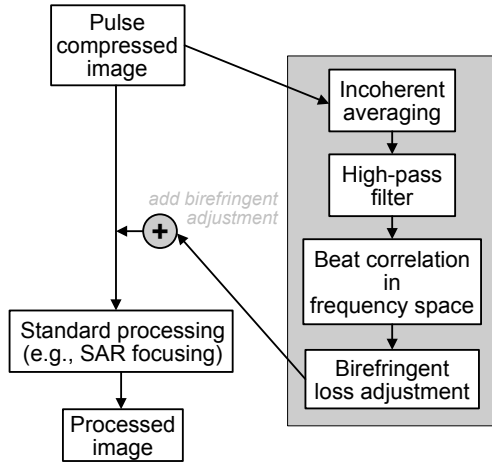


Fig. 3. A flow chart for our birefringent loss correction and its place in the standard processing flow for radar-sounding images.

which expresses the birefringent beat. We then use a high-pass filter in the fast-time dimension to filter the radar power image, removing the low-frequency signal (attenuation).

With the two filtered images, we convolve their signals in the frequency domain, using an expected offset in their beat signature based on their different center frequencies in equation 4. Then, if there is a frequency band in which a highly correlated beat is observed in both signals, that band is artificially suppressed in each. Finally, the beat-suppressed signal is returned to the time domain and the net power difference is applied to the original, unfiltered image. In the COLDEX example (Figure 4), we observe clear beat frequencies at 1.7 and 8.5 km^{-1} in the low and high frequency systems, respectively. The power correction is applied to both signals and effectively removes the dominant beat signature.

V. DISCUSSION AND CONCLUSIONS

We described the physical nature of radar birefringence in ice, the frequency dependence of birefringent power losses, and designed a new birefringence correction applicable for dual- or multi-frequency radar sounding. Since our method leverages two distinct measurements of the same material property, it is robust to noisy signals. In other words, multi-frequency birefringent analyses are feasible among reflectivity variations (e.g., for the reflection at the ice-bed interface) whereas single-frequency analysis is generally not.

Applications of our correction include those for investigations of radar attenuation and interface reflectivity in glaciers and ice sheets which are commonly used to interpret englacial [27, 28] and subglacial [29, 30] properties, respectively. Past studies of attenuation and reflectivity have generally ignored birefringent losses since, in commonly used single-frequency radars, the beat signature cannot always be distinguished from reflectivity variations. Birefringent losses could bias those previous results in cases with anisotropic ice. For example, attenuation estimates which use reflected power from the

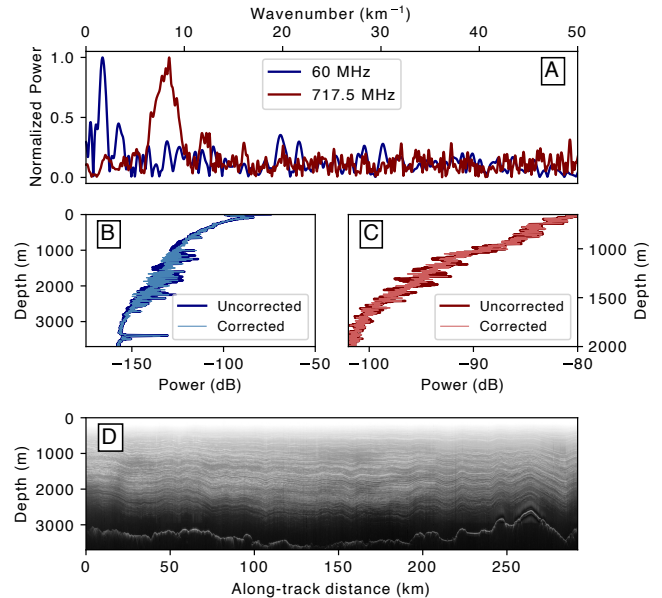


Fig. 4. Radar power correction. A) Frequency spectra for a selected vertical trace (from a selected location at 210 km along track in Figure 2) and for both the 60 MHz and 717.5 MHz instruments. A-scope radar power profiles for both the (B) low and (C) high frequency systems, with the uncorrected trace in a darker thicker line alongside the corrected trace in a lighter thinner line. D) Corrected z-scope image for the 60 MHz instrument.

ice-bed interface assume that the correlation between power and thickness is primarily a result of attenuation [31, 32]; however, as we showed above, birefringent losses vary with thickness (range/depth) as well. In fact, for commonly used radar frequencies and with realistic ice anisotropies, the depth-power gradient is within the range of realistic attenuation rates $\sim 5\text{-}20 \text{ dB/km}$ (e.g., solid black line in Figure 1A). Our method requires an assumption that the ice anisotropy does not change within the vertical depth window over which we infer the birefringent beat, so it may be limited in areas with a strong vertical gradient in crystal fabric.

Multi-frequency birefringence analysis and our power correction also have relevance for radar sounding in planetary environments, although less work has been done on ice anisotropy there. The two radar sounders currently orbiting Mars operate at different frequencies, MARSIS at $1.3\text{-}5.5 \text{ MHz}$ [33] and SHARAD at 20 MHz [34]. Those two instruments are on separate platforms with different orbits, but it could still be feasible to search for birefringent loss correlations between the two in places where anisotropy might be expected to develop in the Martian polar layered deposits. Even more promising, the REASON instrument aboard the Europa Clipper is dual frequency itself, with a low-frequency (6 MHz) and a high-frequency (60 MHz) band [35]. Anisotropy may be expected in Europa's ice shell, based on convection driving COF evolution [36]. If so, a birefringent correction will be necessary for any interpretation of reflected power from beneath the anisotropic ice.

REFERENCES

- [1] P. J. Hudleston, "Structures and fabrics in glacial ice: A review," *Journal of Structural Geology*, vol. 81, pp. 1–27, 2015.
- [2] P. V. Hobbs, *Ice physics*. OUP Oxford, 2010.
- [3] S. Fujita, T. Matsuoka, T. Ishida, K. Matsuoka, and S. Mae, "A summary of the complex dielectric permittivity of ice in the megahertz range and its applications for radar sounding of polar ice sheets," in *Physics of Ice Core Records*. Shikotsukohan, Hokkaido, Japan: Hokkaido University Press, 2000, pp. 185–212.
- [4] S. Fujita, S. Mae, and T. Matsuoka, "Dielectric anisotropy in ice Ih at 9.7 GHz," *Annals of Glaciology*, vol. 17, pp. 276–280, 1993.
- [5] T. Matsuoka, S. Fujita, S. Morishima, and S. Mae, "Precise measurement of dielectric anisotropy in ice Ih at 39 GHz," *Journal of Applied Physics*, vol. 81, no. 5, pp. 2344–2348, 1997.
- [6] R. B. Alley, "Flow-law hypotheses for ice-sheet modeling," *Journal of Glaciology*, vol. 38, no. 129, 1992.
- [7] D. A. Lilien, N. M. Rathmann, C. S. Hvidberg, and D. Dahl-Jensen, "Modeling Ice-Crystal Fabric as a Proxy for Ice-Stream Stability," *Journal of Geophysical Research: Earth Surface*, vol. 126, no. 9, pp. 1–25, 2021.
- [8] M.-G. Llorens, A. Griera, P. D. Bons, I. Weikusat, D. J. Prior, E. Gomez-Rivas, T. de Riese, I. Jimenez-Munt, D. García-Castellanos, and R. A. Lebensohn, "Can changes in deformation regimes be inferred from crystallographic preferred orientations in polar ice?" *The Cryosphere*, vol. 16, no. 5, pp. 2009–2024, 2022.
- [9] Y. Ma, O. Gagliardini, C. Ritz, F. Gillet-Chaulet, G. Durand, and M. Montagnat, "Enhancement factors for grounded ice and ice shelves inferred from an anisotropic ice-flow model," *Journal of Glaciology*, vol. 56, no. 199, pp. 805–812, 2010.
- [10] N. M. Rathmann and D. A. Lilien, "Inferred basal friction and mass flux affected by crystal-orientation fabrics," *Journal of Glaciology*, 2021.
- [11] S. Fujita, H. Maeno, and K. Matsuoka, "Radio-wave depolarization and scattering within ice sheets: A matrix-based model to link radar and ice-core measurements and its application," *Journal of Glaciology*, vol. 52, no. 178, pp. 407–424, 2006.
- [12] T. J. Young, C. Martín, P. Christoffersen, D. Schroeder, S. M. Tulaczyk, and E. J. Dawson, "Rapid and accurate polarimetric radar measurements of ice crystal fabric orientation at the Western Antarctic Ice Sheet (WAIS) Divide ice core site," *Cryosphere*, vol. 15, no. 8, pp. 4117–4133, 2021.
- [13] K. Matsuoka, L. Wilen, S. P. Hurley, and C. F. Raymond, "Effects of birefringence within ice sheets on obliquely propagating radio waves," *IEEE Transactions on Geoscience and Remote Sensing*, vol. 47, no. 5, pp. 1429–1443, 2009.
- [14] A. C. Frémand, P. Fretwell, J. A. Bodart, H. D. Pritchard, A. Aitken, J. L. Bamber, R. Bell, C. Bianchi, R. G. Bingham, D. D. Blankenship *et al.*, "Antarctic bedmap data: Findable, accessible, interoperable, and reusable (fair) sharing of 60 years of ice bed, surface, and thickness data," *Earth System Science Data*, vol. 15, no. 7, pp. 2695–2710, 2023.
- [15] J. A. MacGregor, L. N. Boisvert, B. Medley, A. A. Petty, J. P. Harbeck, R. E. Bell, J. B. Blair, E. Blanchard-Wrigglesworth, E. M. Buckley, M. S. Christoffersen *et al.*, "The scientific legacy of nasa's operation icebridge," 2021.
- [16] V. V. Bogorodskii, C. R. Bentley, and P. Gudmandsen, *Radio-glaciology*. Springer Science & Business Media, 1985, vol. 1.
- [17] S. G. Warren, "Optical constants of ice from the ultraviolet to the microwave," *Applied optics*, vol. 23, no. 8, pp. 1206–1225, 1984.
- [18] F. Rodriguez-Morales, S. Gogineni, C. J. Leuschen, J. D. Paden, J. Li, C. C. Lewis, B. Panzer, D. G.-G. Alvestegui, A. Patel, K. Byers *et al.*, "Advanced multifrequency radar instrumentation for polar research," *IEEE Transactions on Geoscience and Remote Sensing*, vol. 52, no. 5, pp. 2824–2842, 2013.
- [19] E. Collett, *Field guide to polarization*. Bellingham, WA, USA: SPIE, 2005.
- [20] F. T. Ulaby and C. Elachi, *Radar polarimetry for geoscience applications*. Norwood, MA, USA: Taylor & Francis, 1990.
- [21] N. M. Rathmann, D. A. Lilien, A. Grinsted, T. A. Gerber, T. J. Young, and D. Dahl-Jensen, "On the Limitations of Using Polarimetric Radar Sounding to Infer the Crystal Orientation Fabric of Ice Masses," *Geophysical Research Letters*, vol. 49, no. 1, pp. 1–11, 2022.
- [22] T. M. Jordan, D. M. Schroeder, D. Castelletti, J. Li, and J. Dall, "A Polarimetric Coherence Method to Determine Ice Crystal Orientation Fabric from Radar Sounding: Application to the NEEM Ice Core Region," *IEEE Transactions on Geoscience and Remote Sensing*, vol. 57, no. 11, pp. 8641–8657, 2019.
- [23] D. A. Young, J. D. Paden, J. S. Greenbaum, D. D. Blankenship, M. E. Kerr, S. Singh, S. R. Kaundinya, K. Chan, D. P. Buhl, G. Ng, and S. D. Kempf, "COLDEX Open Polar Radar MARFA Airborne Radar Data," 2024. [Online]. Available: <https://doi.org/10.18738/T8/J38CO5>
- [24] E. Brook, "Center for oldest ice exploration annual report," Oregon State University, College of Earth, Ocean, and Atmospheric Sciences, Corvallis, OR, Tech. Rep., 2024.
- [25] T. J. Young, D. M. Schroeder, T. M. Jordan, P. Christoffersen, S. M. Tulaczyk, R. Culberg, and N. L. Bienert, "Inferring Ice Fabric From Birefringence Loss in Airborne Radargrams: Application to the Eastern Shear Margin of Thwaites Glacier, West Antarctica," *Journal of Geophysical Research: Earth Surface*, vol. 126, no. 5, pp. 1–26, 2021.
- [26] T. A. Gerber, D. Lilien, N. Rathmann, S. Franke, T. J. Young, F. Valero-Delgado, R. Ershadi, R. Drews, O. Zeising, A. Humbert, N. Stoll, I. Weikusat, A. Grinsted, C. Hvidberg, D. Jansen, H. Miller, V. Helm, D. Steinhage, C. O'Neill, J. Paden, S. Gogineni, D. Dahl-Jensen, and O. Eisen, "Crystal fabric anisotropy causes directional hardening of the Northeast Greenland Ice Stream," *Nature Communications*, vol. 14, no. 1, p. 2653, 2023.
- [27] W. Chu, D. M. Schroeder, and M. R. Siegfried, "Retrieval of Englacial Firn Aquifer Thickness From Ice-Penetrating Radar Sounding in Southeastern Greenland," *Geophysical Research Letters*, vol. 45, no. 21, pp. 770–11, 2018.
- [28] J. A. MacGregor, J. Li, J. D. Paden, G. a. Catania, G. D. Clow, M. a. Fahnestock, S. P. Gogineni, R. E. Grimm, M. Morlighem, S. Nandi, H. Seroussi, and D. E. Stillman, "Radar attenuation and temperature within the Greenland Ice Sheet," *Journal of Geophysical Research: Earth Surface*, vol. 120, pp. 983–1008, 2015.
- [29] D. M. Schroeder, D. D. Blankenship, and D. a. Young, "Evidence for a water system transition beneath Thwaites Glacier, West Antarctica," *Proceedings of the National Academy of Sciences of the United States of America*, vol. 110, no. 30, pp. 12 225–8, 2013, iISBN: 1091-6490 (Electronic)\r0027-8424 (Linking).
- [30] W. Chu, A. M. Hilger, R. Culberg, D. M. Schroeder, T. M. Jordan, H. Seroussi, D. A. Young, D. D. Blankenship, and D. G. Vaughan, "Multisystem synthesis of radar sounding observations of the amundsen sea sector from the 2004–2005 field season," *Journal of Geophysical Research: Earth Surface*, vol. 126, no. 10, p. e2021JF006296, 2021.
- [31] D. M. Schroeder, H. Seroussi, W. Chu, and D. A. Young, "Adaptively constraining radar attenuation and temperature across the Thwaites Glacier catchment using bed echoes," *Journal of Glaciology*, vol. 62, no. 236, pp. 1075–1082, 2016.
- [32] D. M. Schroeder, C. Grima, and D. D. Blankenship, "Evidence for variable grounding-zone and shear-margin basal conditions across Thwaites Glacier, West Antarctica," *Geophysics*, vol. 81, no. 1, pp. WA35–WA43, 2016.

- [33] G. Picardi, D. Biccari, R. Seu, L. Marinangeli, W. Johnson, R. Jordan, J. Plaut, A. Safaeinili, D. Gurnett, G. G. Ori *et al.*, “Performance and surface scattering models for the Mars Advanced Radar for Subsurface and Ionosphere Sounding (MARSIS),” *Planetary and Space Science*, vol. 52, no. 1-3, pp. 149–156, 2004.
- [34] R. Seu, R. J. Phillips, D. Biccari, R. Orosei, A. Masdea, G. Picardi, A. Safaeinili, B. A. Campbell, J. J. Plaut, L. Marinangeli *et al.*, “SHARAD sounding radar on the Mars Reconnaissance Orbiter,” *Journal of Geophysical Research: Planets*, vol. 112, no. E5, 2007.
- [35] D. D. Blankenship, A. Moussessian, E. Chapin, D. Young, G. Patterson, J. Plaut, A. Freedman, D. Schroeder, C. Grima, G. Steinbrügge, K. Soderlund, T. Ray, T. Richter, L. Jones-Wilson, N. Wolfenbarger, K. Scanlan, C. Gerekos, K. Chan, I. Seker, M. Haynes, A. Barr Mlinar, L. Bruzzone, B. Campbell, L. Carter, C. Elachi, Y. Gim, A. Hérique, H. Hussmann, W. Kofman, W. Kurth, M. Mastrogiovanni, W. McKinnon, J. Moore, F. Nimmo, C. Paty, D. Plettemeier, B. Schmidt, M. Zolotov, P. Schenk, S. Collins, H. Figueiroa, M. Fischman, E. Tardiff, A. Berkun, M. Paller, J. Hoffman, A. Kurum, G. Sadowy, K. Wheeler, E. Decrossas, Y. Hussein, C. Jin, F. Boldissar, N. Chamberlain, B. Hernandez, E. Maghsoudi, J. Mihaly, S. Worel, V. Singh, K. Pak, J. Tanabe, R. Johnson, M. Ashtijou, T. Alemu, M. Burke, B. Custodero, M. Tope, D. Hawkins, K. Aaron, G. Delory, P. Turin, D. Kirchner, K. Srinivasan, J. Xie, B. Ortloff, I. Tan, T. Noh, D. Clark, V. Duong, S. Joshi, J. Lee, E. Merida, R. Akbar, X. Duan, I. Fenni, M. Sanchez-Barbetty, C. Parashare, D. Howard, J. Newman, M. Cruz, N. Barabas, A. Amirahmadi, B. Palmer, R. Gawande, G. Milroy, R. Roberti, F. Leader, R. West, J. Martin, V. Venkatesh, V. Adumitroaie, C. Rains, C. Quach, J. Turner, C. O’Shea, S. Kempf, G. Ng, D. Buhl, and T. Urban, “Radar for Europa Assessment and Sounding: Ocean to Near-surface (REASON),” *Space Science Reviews*, vol. 220, no. 5, p. 51, 2024.
- [36] M. Rudolph and M. Manga, “Effects of anisotropic viscosity and texture development on convection in ice mantles,” *Journal of Geophysical Research: Planets*, vol. 117, no. E11, 2012.